

Joint Sensor Deployment and Physics-Informed Graph Transformer for Smart Grid Attack Detection

Mariam Elnour¹, Mohammad AlShaikh Saleh², Rachad Atat³, Xiang Huo⁴, Abdulrahman Takiddin⁵,
Muhammad Ismail⁶, Hasan Kurban⁷, Katherine R. Davis¹, Erchin Serpedin¹

Abstract—This paper proposes a joint multi-objective optimization framework for strategic sensor placement in power systems to enhance attack detection. A novel physics-informed graph transformer network (PIGTN)-based detection model is proposed. Non-dominated sorting genetic algorithm-II (NSGA-II) jointly optimizes sensor locations and the PIGTN’s detection performance, while considering practical constraints. The combinatorial space of feasible sensor placements is explored using NSGA-II, while concurrently training the proposed detector in a closed-loop setting. Compared to baseline sensor placement methods, the proposed framework consistently demonstrates robustness under sensor failures and improvements in detection performance in seven benchmark cases, including the 14, 30, IEEE-30, 39, 57, 118 and the 200 bus systems. By incorporating AC power flow constraints, the proposed PIGTN-based detection model generalizes well to unseen attacks and outperforms other graph network-based variants (topology-aware models), achieving improvements up to 37% in accuracy and 73% in detection rate, with a mean false alarms rate of 0.3%. In addition, optimized sensor layouts significantly improve the performance of power system state estimation, achieving a 61%–98% reduction in the average state error.

Index Terms—Genetic algorithm, graph transformer network, physics-informed neural networks, sensor placement

I. INTRODUCTION

Power systems are becoming increasingly vulnerable to cyber-physical threats due to the rapid integration of new emerging smart grid technologies, such as advanced metering infrastructure, monitoring devices, microgrids, electric vehicles and charging units, cyber-physical energy systems and decentralization of energy trading and market. Undiscovered system vulnerabilities, if exploited by adversaries, can have a

significant impact, such as the famous Ukrainian power grid blackout that took place in 2015 [1]. However, when used effectively and combined with artificial intelligence (AI), the sensor infrastructure can be used to enhance monitoring and defense strategies [2]. Using historical sensor data, numerous data-driven attack detection methods were studied [3].

Specifically, most recent works used graph neural networks (GNNs) extensively for attack detection in power systems and demonstrated notable performance. For instance, a spatio-temporal wavelet graph convolutional neural network (GCN) was presented in [4] to localize dummy false data injection attacks (FDIAs). In [5], spectral GCNs were proposed to support bad data detectors (BDDs) in stealthy FDIA detection. For greater flexibility and representational power, graph transformer-based models represent promising solutions, motivated by the outstanding performance observed of transformers in natural language processing [6] and computer vision [7], along with the demonstrated value of GNNs as topology-aware models [8]. Graph transformers incorporate graph inductive bias (prior knowledge or assumptions about graph properties) to effectively process graph data [7]. They possess the capability to handle dynamic and heterogeneous graphs, and to adapt to changing network structures.

Nevertheless, despite the remarkable results acquired by graph-based models, they are susceptible to poor extrapolation capabilities, scalability constraints, and the explainability of the system’s physical laws. Without embedding these laws, model predictions are mostly black-box outputs. Such limitations reduce their reliability as power system operators often face problems in interpreting their implications. To avoid such problems, physics-informed neural networks (PINNs) were introduced, integrating the fundamental physical principles of systems into neural network (NN) models [9]. Extending this idea to graph transformer networks (GTNs), they can be enhanced to capture long-range dependencies with improved interpretability by integrating physics-informed design. However, the reliability of such models is still contingent on the quality and scope of their input data.

This highlights a critical dependency between modeling and sensing. Even for advanced models such as physics-informed graph transformer networks (PIGTNs), their performance is fundamentally bounded by the representativeness of the data used in model training and operation. Existing work using data-driven detection methods in power systems often assumes that sensors are available at all nodes, overlooking the significant impact of sensor placement on detection efficacy. This assumption simplifies modeling and does not reflect real-world

¹ M. Elnour, K. R. Davis, and E. Serpedin are with the department of Electrical and Computer Engineering, Texas A&M University, College Station, TX 77840, USA. (email: melnour@tamu.edu, katedavis@tamu.edu, eserpedin@tamu.edu)

² M. A. Saleh is with the department of Electrical and Computer Engineering, Texas A&M University at Qatar, Doha, Qatar. (email: mohamad.saleh@qatar.tamu.edu)

³ R. Atat is with the department of Computer Science and Mathematics, Lebanese American University, Beirut 1102-2801, Lebanon. (email: rachad.atat@lau.edu.lb)

⁴ X. Huo is with the department of Electrical and Computer Engineering, Hampton University, 100 E Queen St, Hampton, VA 23669, USA (email: xiang.huo@hamptonu.edu)

⁵ A. Takiddin is with the department of Electrical and Computer Engineering, FAMU-FSU College of Engineering, Florida State University, 2525 Pottsdamer Street, Tallahassee, FL 32310-6046, USA. (email: a.takiddin@fsu.edu)

⁶ M. Ismail is with the Cybersecurity Education, Research, and Outreach Center (CEROC) and the department of Computer Science, Tennessee Tech University, Cookeville, TN, USA. (email: mismail@tntech.edu)

⁷ H. Kurban is with the College of Science and Engineering, Hamad Bin Khalifa University, Doha 34110, Qatar. (email: hkurban@hbku.edu.qa)

scenarios where sensor deployment may be less extensive due to budgetary, logistic, and other practical constraints. This dual perspective motivates this work where PIGTNs provide a principled means to model and detect complex attacks with improved reliability, while joint sensor deployment ensures that the model receives representative and physically meaningful data to operate effectively.

A. PINNs in Power Systems

PINNs, a branch of scientific machine learning, combined data-driven and physics-driven approaches to solve science and engineering problems [9], [10]. These PINN models utilized prior knowledge of physics through algebraic (less common) and differential equations that explain the relationship among the variables in the given data. The role of PINNs in cyber attack detection in power systems is still emerging. According to [11], PINNs were used for state/parameter estimation, dynamic analysis, power flow calculation/voltage prediction, optimal power flow applications, and fault diagnosis. However, no studies have yet comprehensively researched PINN-based cyber-attack detection, especially in the case of different types of attacks imposed on various network topologies. In [12], a physics-informed convolutional autoencoder (PIConvAE) was applied to detect FDIAs in power distribution grids. Although promising performance was achieved, the study lacked comprehensive benchmark evaluations as it was evaluated on two test cases, the IEEE 13-bus and 123-bus systems, and against a single benchmark detector.

To address this gap, this paper presents a comprehensive evaluation of the PIGTN—a physics-informed graph-aware data-driven model, that integrates the physics-based relationships of phasor measurements into the graph-based detection model. To the best of the authors’ knowledge, we propose the first PIGTN-based cyber-attack detector for power systems. The proposed PIGTN leverages the graph transformer network (GTN) to process graph-structured data of the electrical topologies while enhancing explainability due to encoding the physical laws, i.e., the AC power flow equations, as a regularization term in the loss function, resulting in physically consistent predictions.

B. Sensor Placement in Power Systems

Traditionally, the sensor placement problem was studied in the context of system observability for power system state estimation (PSSE) and energy management system (EMS) functions [21]–[23]. Early works employed optimization techniques including integer linear programming (ILP) [24]–[26], greedy algorithms [27], and evolutionary algorithms [28], [29] to ensure minimal-cost deployments. They focused almost exclusively on achieving topological or numerical observability. However, adversaries could craft attacks that precisely exploit this fully observable structure to remain hidden from conventional detection schemes. Additionally, when measurements are concentrated on specific buses or are unevenly spread across the network, attackers may leverage this setting to manipulate poorly monitored subsets of the available sensor network and achieve their goal. Consequently, a placement

strategy that satisfies observability alone may not guarantee attack–resilience, a gap that is not addressed enough in the literature.

Recent works explored optimal sensor placement for fault or anomaly detection (Table I). For instance, a strategic phasor measurement unit (PMU) placement strategy using ILP was proposed in [13] to maximize the performance of model-based sparse estimation-based line outage and fault diagnosis. The study in [14] focused on PMUs placement for wide-area backup protection such that every line fault was detectable based on voltage path differences. In [15], a PMU placement strategy was presented for a near-optimal resolution to localize faults given the limitations of available PMUs using graph signal sampling. An ILP sensor placement problem was reported in [16] that aimed to minimize the number of PMUs, incorporating phase observability constraints to ensure components needed for diagnosis were measured. Then a neural network was developed for the diagnosis of the fault followed by an ensemble algorithm for the precise localization of the line level. In [17], a hierarchical anomaly detection framework for distribution grids was proposed, combining optimally placed PMUs with physics-informed local and central detection rules to identify deviations from quasi-steady-state operation. These strategies improved fault and anomaly detection; however, such anomalies are not necessarily cyber-attacks, and attacks can remain undetected by methods designed only for faults or random anomalies [30]. Additionally, they were mainly model-based, and for the data-driven methods, the sensor placement was optimized separately from the detection model.

A second category of works optimized sensor placement specifically to improve attack detection. The authors in [19] studied the performance of FDIA subspace projection detection (SPD) given the problem of PMU placement. The optimization aimed to place PMUs in order to minimize the energy retained in the normal (healthy) subspace. In [20], a greedy PMU placement strategy was proposed to improve the performance of PSSE, by deploying PMUs that maximally protect the most vulnerable measurements. A pre-deployment PMU-based greedy algorithm was proposed in [18] that aimed first to protect attack-vulnerable buses, then iteratively added further PMUs until numerical observability was achieved. These methods present a critical limitation: they are model-based, which may be ineffective against sophisticated attacks that align with the models used.

Notably, none integrated the placement optimization directly with data-driven detection models. Our proposed framework bridges this gap by jointly optimizing sensor placement and detection performance. It aims to explicitly address the interplay between data-driven detection models, specifically graph-based, and sensor network in power systems. It addresses the fundamental problem of detection capability of graph learning models in the presence of practical constraints.

C. Contributions

We propose a joint optimization framework that simultaneously considers sensor placement and attack detection. It integrates both in a single, multi-objective optimization

TABLE I: Summary of related works in sensor placement for power systems.

Ref	Task	Diagnosis Model	Optimization	Objective Function	Constraints	Joint or Standalone?
[13]	Line fault detection	Model- and Data-based	ILP	Min. number of PMUs	Coverage	Joint (model-based), Standalone (data-driven)
[14]	Line fault detection	Model-based	ILP	Min. number of PMUs	Coverage, Redundancy	Standalone
[15]	Line fault localization	Model-based	Greedy	Min. influence of unmeasured on measured buses	N/A	Joint to increase fault localization resolution
[16]	Fault diagnosis	Data-driven	ILP	Min. number of PMUs	Topological observability	Standalone
[17]	Anomaly detection	Rule-based	Min–Max	Min. max eigenvalue of sensitivity matrix	Placement feasibility	Standalone
[18]	FDIA detection	Model-based	Greedy	Min. number of PMUs	Numerical observability	Joint with state estimation
[19]	FDIA detection	Model-based	Greedy	Min. projection energy in normal subspace	N/A	Joint to improve SPD-based detection
[20]	FDIA defense	Model-based	Greedy	Max. resilience of state estimation	N/A	Joint for stealthy FDIA defense

process instead of treating these tasks in isolation. We employ Genetic Algorithm (GA) to explore the combinatorial space of feasible sensor placements under relevant constraints [31], and concurrently train the attack detection model in a closed-loop setting. The framework solves for an optimized sensor layout that ensures an effective trade-off between detection performance and sensor placement objectives.

In summary, our contributions are as follows:

- We address the connection between sensor placement and data-driven attack detection in power systems by jointly optimizing these two problems. The proposed framework combines constrained GA-based sensor placement with supervised attack PIGTN-based detection. We propose a hybrid node importance score that integrates both topological and electrical characteristics of the power network. This score guides the GA initialization and mutation processes to promote a more effective exploration–exploitation balance. It results in optimized sensor layouts for improved overall detection performance.
- We incorporate governing physical laws (AC power flow equations) into the proposed model’s loss function, guiding the predictions to remain consistent with the real-world constraints of the system rather than relying merely on statistical correlations in the data. Our benchmarking evaluation considers seven other robust topology-aware detectors using 14, 30, IEEE-30, 39, 57, 118, and 200 bus systems. The proposed framework shows strong generalization to unseen attacks during testing. Compared to benchmark detectors, our PIGTN consistently achieves superior performance. On average, the proposed PIGTN outperforms the best-performing baselines with an average F1-score of 93% across all cases, and a mean FPR of 2%, providing performance improvements ranging from 2.23%–27.5% (averaged across all seven bus system cases) relative to the state-of-the-art topology-aware graph models.
- Our proposed framework consistently outperforms benchmark placement methods across the seven test cases. Detection rate improvements are case-dependent, ranging from mixed to around 7%. The varied improvements reflect the influence of network functional and structural characteristics, while false alarm rates are maintained at comparable or lower levels. More importantly, under sensor failures, the framework yields the most robust sensor layouts. Specifically, GA-PIGTN achieves higher robustness scores (up to 0.907), and superior average accuracy (4.8% improvement vs. 3% for benchmarks), F1-score (2.6% vs. 1.3–1.6%), and precision (6.5% vs.

3.2–3.7%) across varied sensor failure levels.

- In addition to enhancing attack detection, the optimized sensor layout leads to improved PSSE performance in all test cases, with 61% to 94% reduction in voltage magnitude error and 77% to 98% reduction in voltage angle error, evaluated on the weighted least squares (WLS) state estimator.

The rest of the paper is organized as follows. Section II outlines attack models considered in this work. The problem formulation is presented in Section III, and the details of the optimization methodology and proposed PIGTN detector are presented in Section IV. Section V presents the experimental results, performance comparisons, and discussion. Finally, Section VI concludes the paper and suggests directions for future research.

II. ATTACK MODELING

The attack modeling focuses on FDIAs, where an adversary strategically manipulates or injects false data into the system to compromise its integrity, accuracy, or functionality. It is a critical attack as it can result in mislead monitoring, decision-making, or control processes [32]–[34]. This class of FDIAs are crafted from normal measurement data [35].

1) *Random Attack*: The measurement data is perturbed slightly. The alteration is modeled as a small perturbation factor α , which is applied uniformly across the benign samples. The adversarial measurement $Z_s(t, i)$ at timestamp t and bus i is generated by [35]: $Z_s(t, i) = (1 + \alpha)Z_b(t, i)$, where $Z_b(t, i)$ is the original benign measurement.

2) *General Attack*: It introduces larger, more systematic changes to the measurement data. It manipulates the data according to [35]: $Z_s(t, i) = Z_b(t, i) + (-1)^\beta \alpha \gamma \text{Range}(Z_b(i))$, where β is a binary random variable, α is the attack magnitude, γ is a uniform random variable between 0 and 1, and $\text{Range}(\cdot)$ denotes the range of the measurement.

3) *Load Redistribution (LR) Attacks*: They are a class of cyber-attacks that redistribute loads among the buses while keeping the net load unchanged. The false loads in an LR attack satisfy [36], [37]: $Z_s(t, i) = Z_b(t, i) + \Delta Z(t, i)$, $\sum_i \Delta Z(t, i) = 0$, where ΔZ is the load change caused by the attack. The *load shift* τ quantifies the attack’s detectability and is defined as the largest load change in percentage of the true loads: $\tau = \max_i \left| \frac{\Delta Z(t, i)}{Z_b(t, i)} \right| \times 100\%$. Attacks with large τ are easily detectable, so adversaries’ typical limit is $\tau \leq 20\%$.

III. PROBLEM FORMULATION

The sensor placement problem is formulated as a constrained multi-objective optimization problem. The goal is to minimize the number of installed sensors and to simultaneously enhance graph-based attack detection performance. Non-dominated sorting genetic algorithm II (NSGA-II) is used because it maintains solution diversity and effectively balances competing objectives [38]. The formal optimization formulation is described in the following subsections.

1) *Decision Variables*: The decision variable is the binary vector, $X = [x_1, x_2, \dots, x_{N_c}]$, $x_i \in \{0, 1\}$, where N_c is the number of candidate nodes for sensor placement, and $x_i = 1$ indicates a sensor is placed at node i , and $x_i = 0$ otherwise.

2) *Objectives*: The multi-objective optimization problem is formulated as:

$$\begin{aligned} \min_X (f_1(X) + f_2(X)) \\ \text{s.t. } V \leq \varepsilon, \end{aligned} \quad (1)$$

where $f_1(X) = \sum_{i=1}^{N_c} x_i$ is the number of sensors [31] and $f_2(X) = \mathcal{L}(y_k, \hat{y}_k)$ is the detection performance cost, with $\mathcal{L}(\cdot)$ as the model loss function, y_k as the true labels, and \hat{y}_k as the predicted labels. The optimization incorporates requirements related to sensor layout's connectivity, coverage, and redundancy. A total constraints violation (V) is defined as: $V = w_{cn}P_{\text{connectivity}} + w_{cr}P_{\text{coverage}} + w_{rd}P_{\text{redundancy}}$, representing the weighted aggregated violations of individual constraints, where w_{cr} , w_{rd} , w_{cn} denote connectivity, coverage, and redundancy violation weights, respectively, and ε stands for the constraints violation tolerance. For a power network modeled as a graph $\mathcal{G} = (\mathcal{V}, \mathcal{E})$, where \mathcal{V} indicates the buses and \mathcal{E} represents the transmission lines or transformers, the requirements are the following:

a) *Connectivity*: Let $\mathcal{S} = \{i \in \mathcal{V} | x_i = 1\}$ be the set of sensor-equipped nodes and $\mathcal{E}_{\mathcal{S}}$ be the active edges. It is desirable for the sensor network to form a connected graph, $\mathcal{G}_{\mathcal{S}}$, to provide the graph-based detection model with a well-connected receptive field message passing [39]. A virtual flow-based formulation is used (Eq. (2)), where a single flow is initiated at a selected root node $k \in \mathcal{S}$ and must reach all other selected nodes through activated edges. The connectivity constraints are defined as:

$$\begin{aligned} \sum_{j \in \mathcal{N}(k)} f_{kj} &= \sum_{\substack{i \in \mathcal{V} \\ i \neq k}} x_i \\ \sum_{j \in \mathcal{N}(i)} f_{ji} - \sum_{j \in \mathcal{N}(i)} f_{ij} &= -x_i, \quad \forall i \in \mathcal{V} \setminus \{k\} \\ 0 \leq f_{ij} &\leq (|\mathcal{V}| - 1) \cdot y_{ij}, \quad \forall (i, j) \in \mathcal{E} \\ y_{ij} &\leq x_i, \quad y_{ij} \leq x_j, \quad \forall (i, j) \in \mathcal{E} \end{aligned} \quad (2)$$

where f_{ij} denotes the virtual flow between nodes i and j , and y_{ij} is a binary indicator for edge activation. The constraint violation term is defined via $P_{\text{connectivity}} = 1$ if \mathcal{S} is disconnected, and 0 otherwise. A binary formulation is used to impose strict satisfaction of the connectivity requirement without allowing partial feasibility.

b) *Coverage*: This constraint is to promote r -hop coverage of nodes [31], with critical nodes prioritized. It aims to encourage critical nodes visibility to the detection model, either directly equipped with a sensor or sufficiently covered

by neighbors within r -hop reach. Each node j is said to be covered if there exists at least one sensor within its r -hop neighborhood:

$$\text{coverage}(j) = \begin{cases} 1, & \text{if } \sum_{i \in \mathcal{N}_r(j)} x_i \geq 1 \\ 0, & \text{otherwise} \end{cases} \quad (3)$$

where $\mathcal{N}_r(j) = \{i \in \mathcal{V} | d(i, j) \leq r\}$ is the r -hop neighborhood of node j , i.e., the set of nodes that can cover node j within a coverage radius r , and $d(i, j)$ is the topological distance between nodes i and j , computed using the Breadth-First Search (BFS) algorithm. The corresponding penalty is computed as: $P_{\text{coverage}} = \frac{1}{N_c} \sum_{j=1}^{N_c} \alpha_j (1 - \text{coverage}(j))$, where α_j is the criticality weight of node j .

c) *Redundancy*: A single-sensor coverage may be insufficient to guarantee robustness against failures. Hence, a redundancy constraint is used to encourage nodes being monitored by multiple sensors [31]. Introducing $u_j = \sum_{i \in \mathcal{N}_r(j)} x_i$, the violation is expressed as: $P_{\text{redundancy}} = \frac{1}{N_c} \sum_{j=1}^{N_c} \max(R_{\min} - u_j, 0)$, where R_{\min} is the minimum redundancy requirement.

IV. PROPOSED JOINT OPTIMIZATION FRAMEWORK

A. Optimization Methodology Using NSGA-II

The sensor placement strategy follows a principled approach that accounts for the criticality of nodes within the power network. We propose a hybrid population initialization strategy tailored for this placement optimization problem (Algorithm 1). It aims to generate a diverse and high-quality set of initial candidate solutions, each representing a valid configuration of sensors placed on a subset of network buses. It combines domain-driven heuristics with diversity-aware random sampling that improves search efficiency. The initialization strategy starts with heuristic seeding in which a fraction of the population is initialized using top- K selection based on importance scores and greedy coverage to maximize observability within a predefined radius. Then additional individuals are generated randomly, but only accepted if they meet a minimum Hamming distance threshold from existing solutions. Remaining individuals are filled using random sampling to reach the desired population size.

Mutation operations within NSGA-II are guided by node importance (Algorithm 2), with the probability checks applied sequentially to implement independent random draws at each stage, and preserve stochastic diversity in the search process. Non-dominated sorting and crowding distance measures guide selection towards diverse, high-quality solutions. Offspring replace parent solutions based on Pareto dominance and solution diversity metrics, iterating until convergence. NSGA-II sorts the joint parent-offspring population into Pareto fronts based on dominance; within each front, individuals are ranked by crowding distance, thus preserving a diverse approximation to the Pareto optimal set without requiring any user-defined objective weights. The constraints are handled via Deb's constraint-domination principle [40]. In NSGA-II each individual is evaluated on three objectives: (V, f_1, f_2) .

During non-dominated sorting, NSGA-II treats V as the *first* objective to minimize such that fully feasible solutions

Algorithm 1 Hybrid population initialization

Require: graph \mathcal{G} , eligible nodes $\mathcal{V}_{\text{eligible}}$, importance scores S_I , population size N_{pop} , maximum number of sensors K , coverage radius r , heuristic fraction h_{frac} , diversity fraction d_{frac} , Hamming threshold d_{min} .

Ensure: Initialize empty population $\mathcal{P} \leftarrow \emptyset$, $N_c \leftarrow |\mathcal{V}_{\text{eligible}}|$.

- 1: Compute descending order of importance scores $S_I \rightarrow S_{I \text{ sorted}}$
- 2: **for all** $i \leftarrow 1$ to $\lfloor h_{\text{frac}} \cdot N_{\text{pop}}/2 \rfloor$ **do**
- 3: Select top- K nodes from $S_{I \text{ sorted}}$, apply tie-breaking if needed
- 4: Add to \mathcal{P} if unique
- 5: **end for**
- 6: **for all** $i \leftarrow 1$ to $\lfloor h_{\text{frac}} \cdot N_{\text{pop}}/2 \rfloor$ **do**
- 7: Apply greedy r -hop coverage from $\mathcal{V}_{\text{eligible}}$
- 8: Add to \mathcal{P} if unique
- 9: **end for**
- 10: **while** $|\mathcal{P}| < (h_{\text{frac}} + d_{\text{frac}}) \cdot N_{\text{pop}}$ **do**
- 11: Randomly select $\leq K$ nodes from $\mathcal{V}_{\text{eligible}}$
- 12: Construct binary vector \mathbf{X}
- 13: **if** $\text{Hamming}(\mathbf{X}, \mathcal{P}) \geq d_{\text{min}} \cdot N_c$ **then**
- 14: Add \mathbf{X} to \mathcal{P}
- 15: **end if**
- 16: **end while**
- 17: **while** $|\mathcal{P}| < N_{\text{pop}}$ **do**
- 18: Randomly select $\leq K$ nodes from $\mathcal{V}_{\text{eligible}}$
- 19: Add to \mathcal{P} if unique
- 20: **end while**
- 21: **return** Population \mathcal{P} of binary vectors

Algorithm 2 Biased mutation

Require: binary vector \mathbf{X} , importance scores S_I , mutation probability indpb , probability of importance-based flip b_F .

Ensure: $\text{FlipBit}(\cdot)$ be a random flip function, and $\text{UniRand}(0, 1)$ be a uniformly-distributed random number generator function.

- 1: **for all** $i \leftarrow 1$ to $\text{length}(\mathbf{X})$ **do** ▷ Nested mutation prob. logic
- 2: **if** $\text{UniRand} < \text{indpb}$ **then** ▷ 1. Main Mutation prob. logic
- 3: **if** $\text{UniRand} < b_F$ **then** ▷ 2. Importance-based logic
- 4: **if** $\text{UniRand} < I[i]$ **then** ▷ 3. Importance-based flip
- 5: $\mathbf{X}[i] \leftarrow 1$
- 6: **else**
- 7: $\mathbf{X}[i] \leftarrow 0$
- 8: **end if**
- 9: **else**
- 10: $\mathbf{X}[i] \leftarrow \text{FlipBit}(\mathbf{X}[i])$ ▷ Flip randomly otherwise
- 11: **end if**
- 12: **end for**
- 13: **return** Mutated \mathbf{X}

dominate infeasible ones and among infeasible solutions, dominance is determined by the degree of constraint violation. At termination, the Pareto front may contain both feasible ($V_i = 0$) and infeasible ($V_i > 0$) trade-offs. We select our final champion as follows: $\text{best} = \min_{i \in \text{front}} (\mathbb{I}(V_i > 0), V_i, f_{1,i} + f_{2,i})$. The selection process goes as follows: (i) all feasible solutions rank ahead of any infeasible, (ii) among infeasible, the one with smallest V_i is preferred, and (iii) within the chosen class (all with equal first two values), the individual with minimal $f_{1,i} + f_{2,i}$ is selected. In this setup, ε is not explicitly predefined; its effective value emerges from the final Pareto front, being either zero when feasible solutions exist or equal to the smallest V_i among the infeasible solutions selected according to the defined ranking process.

B. Node Importance Metric

To identify critical buses in the power system network, we utilize a hybrid node importance score that combines both *topological* and *electrical* centrality metrics. For each

bus $v \in \mathcal{V}$, the importance score $S_I(v)$ is computed as a weighted sum of individually normalized centrality values: $S_I(v) = w_{\text{bc}} \hat{C}_{\text{B}}(v) + w_{\text{eic}} \hat{C}_{\text{EI}}(v) + w_{\text{ebc}} \hat{C}_{\text{EBC}}(v) + w_{\text{ecd}} \hat{C}_{\text{ECD}}(v)$, where $\hat{C}_i(v) = C_i(v) / \max(C_i)$ is the normalized centrality score for metric i , and w_i is the corresponding weight, chosen empirically based on ablation study results, satisfying $\sum w_i = 1$. These metrics are defined as follows:

1) *Topological Centrality Metrics*: These metrics capture the structural role of buses [41], and quantify node criticality based on graph connectivity. We employ: (i) Betweenness centrality which measures the extent to which a node lies on paths between other nodes. For a node v , it is given by: $C_{\text{B}}(v) = \sum_{s \neq v \neq t} \frac{\sigma_{st}(v)}{\sigma_{st}}$, where σ_{st} denotes the total number of shortest paths from node s to node t , and $\sigma_{st}(v)$ stands for the number of those paths that pass through node v . In this context, it highlights buses that act as structural bridges or bottlenecks. (ii) Eigenvector centrality that measures node's influence within a network, where connections to more central nodes contribute more to the score. It identifies buses with widespread topological influence, even if they do not have many direct connections. It is expressed as: $C_{\text{EI}}(v) = \frac{1}{\lambda} \sum_{k \in \mathcal{N}(v)} C_{\text{EI}}(k)$, where λ is the largest eigenvalue of the adjacency matrix, and $\mathcal{N}(v)$ is the set of neighbors of node v .

2) *Electrical Centrality Metrics*: These metrics capture the physical and operational roles of buses in the power system [42]–[44]. We utilize two complementary metrics, for power transfer roles and for electrical coupling and proximity: (i) Electrical betweenness centrality, which accounts for actual power flow by quantifying the participation of a node in power transfers between generator-load pairs. It helps to identify buses that serve as key power conduits across the network. The following notations will be used: G for the set of generator nodes, L for the set of load nodes, W_i for the rated generation capacity of generator i , W_j for the actual or peak load at load node j , $B_e(n) = \sum_{i \in G, j \in L} \sqrt{W_i W_j} B_{e,ij}(n)$, where $B_{e,ij}(n)$ is the electrical betweenness of node n under unit injection between node pair (i, j) , defined as,

$$B_{e,ij}(n) = \begin{cases} \frac{1}{2} \sum_m |I_{ij}(m, n)|, & n \neq i, j \\ 1, & n = i \text{ or } j, \end{cases}$$

m is a node directly connected to n , and $I_{ij}(m, n)$ is the current in link (m, n) under unit injection between i and j . The normalized electrical betweenness centrality is expressed as: $C_{\text{EBC}}(v) = \frac{B_e(v)}{\sum_{i \in G, j \in L} \sqrt{W_i W_j}}$, and (ii) Electrical coupling connection degree, which represents electrical closeness using the resistance distance derived from the impedance matrix $Z_{\text{bus}} = Y_{\text{bus}}^{-1}$. It measures how easily a node can reach or influence others in the network, i.e., electrically well-integrated buses that can quickly affect or respond to system changes. It is expressed as: $C_{\text{ECD}}(v) = \frac{1}{\sum_{u \neq v} (Z_{vv} + Z_{uu} - 2Z_{vu})}$.

C. Proposed Detectors: Physics-Informed GNN-based Models

Given N buses for different power network topologies, the following measurements are acquired for each bus i

$$\mathcal{X}_i = [V_i, I_i, \theta_i, \delta_i, P_i, Q_i], \quad (4)$$

where V_i and I_i denote voltage and current magnitudes, θ_i and δ_i stand for voltage and current phase angles, and P_i and

Q_i represent active and reactive power measurements, respectively. In our forward modelling case, PINN is leveraged as a conventional numerical solver approach. Therefore, we assume that the unknown $u(\mathcal{X}, t)$ is obtained by an *ansatz* $u(\mathcal{X}, t; \mathbf{w})$, consisting of the proposed GNN-based network with input features $\mathcal{X} = (x_1, \dots, x_d)$ in the domain $\mathcal{X} \in \Omega \subset R^d$, time t incorporates the temporal correlations within the domain $[0, T]$ and weights \mathbf{w} of the graph-based network. The open set $\Omega \subset R^d$ represents the physical domain, and $u: \Omega \cup \partial\Omega \rightarrow R$ is a physical quantity, with $\partial\Omega$ as the boundary of Ω . The objective is to obtain network weights \mathbf{w} such that [10]

$$\mathcal{F}(u(\mathcal{X}, t; \mathbf{w}), \mathcal{X}, t, Du(\mathcal{X}, t; \mathbf{w}), D^2u(\mathcal{X}, t; \mathbf{w}), \dots), \quad (5)$$

$$D^k u(\mathcal{X}, t; \mathbf{w}); \phi) = f(\mathcal{X}, t). \quad \mathcal{X}, t \in \Omega.$$

Equation (5) represents a general partial differential equation (PDE) of order k , where \mathcal{F} is the given function for the problem at hand, $f(\mathcal{X}, t)$ is the forcing function, and the equation must be satisfied at all $\mathcal{X}, t \in \Omega$. The partial derivatives of the GNN-based network output for \mathcal{X} and \mathbf{w} at time t in \mathcal{F} are calculated using automatic-differentiation (AutoDiff) methods. They are described collectively by $D^\alpha u(\mathcal{X}, t; \mathbf{w})$, which is the set of all the partial derivatives of u of order α :

$$D^\alpha u(\mathcal{X}, t; \mathbf{w}) = \left\{ \frac{\partial^\alpha u}{\partial x_1^{\alpha_1} \dots \partial x_d^{\alpha_d}} \mid \alpha_1 + \dots + \alpha_d = \alpha \right\}. \quad (6)$$

AutoDiff is a computational method that allows to obtain the exact derivatives in an efficient manner.

In this work, an additional loss term is added to the GNN variants' loss function to constrain their outputs to satisfy the physics-driven laws (Kirchhoff's laws). For the data obtained from each bus (vector \mathcal{X} in Equation (4)), the outputs should be in line with Kirchhoff's laws at each node and at each time slot t . This approach offers the advantage of identifying whether an attack is present or not along with the different types of attacks present at a given network topology, satisfying the physics-based relationships between measurements for the power flow calculations. Therefore, the physics-driven loss functions for the measurements at bus i are defined as

$$\mathcal{L}_P(\hat{\mathcal{X}}) = \frac{1}{N} \sum_{k=1}^N \left| \hat{P}_i^k - \hat{V}_i^k \hat{I}_i^k \cos(\hat{\theta}_i^k - \hat{\delta}_i^k) \right|^2 \quad (7)$$

$$\mathcal{L}_Q(\hat{\mathcal{X}}) = \frac{1}{N} \sum_{k=1}^N \left| \hat{Q}_i^k - \hat{V}_i^k \hat{I}_i^k \sin(\hat{\theta}_i^k - \hat{\delta}_i^k) \right|^2, \quad (8)$$

where $\mathcal{L}_P(\hat{\mathcal{X}})$ and $\mathcal{L}_Q(\hat{\mathcal{X}})$ are the deviations of the outputs from P and Q in the AC power flow equations, respectively. The total function for training the PIGNN models is created by combining the data and physics loss functions as

$$\mathcal{L}_T(W, b, \mathcal{X}, \hat{\mathcal{X}}) = \lambda_{\text{Data}} \mathcal{L}_{\text{Data}} + \lambda_{\text{Phy}} (\mathcal{L}_P + \mathcal{L}_Q), \quad (9)$$

where λ_{Data} and λ_{Phy} denote the data-driven and physics-based loss coefficients. Such regularization ensures the balance between the loss terms. Through hyperparameter searching, λ_{Data} was set to 1 and λ_{Phy} to 0.2.

V. EXPERIMENTAL EVALUATION

The proposed framework is evaluated on a power system already observable under its existing metering infrastructure that it is intended to supplement. In baseline sensor layouts, *generator buses* are equipped with voltage magnitude $|V|$

and active-power injection P measurements, (ii) *load buses* provide active- and reactive-power injections (P, Q) readings, obtained either from dedicated meters or high-quality pseudo-measurements, and (iii) *the slack (reference) bus* has voltage phasor $|V| \angle \delta$ together with active-power injection P [45]. The data used in the development and evaluation phase covers attack scenarios varying in the percentage of targeted buses. The training dataset contains random and general attack events, and a 70% vs. 30% split is used for the training and validation sets. A dedicated test dataset is collected for various unseen LR attack scenarios. The detection performance is evaluated using the following metrics, accuracy (ACC), true positive rate (TPR), false positive rate (FPR), precision (PREC), and F1-score. The settings used for the optimization methodology are as follows: N_{pop} of 20–50, b_F of 0.8, indpd of 0.1, K as 30% of number of buses, h_{frac} of 0.2, d_{frac} of 0.3, and d_{min} of 0.1–0.3. The constraints violations are given equal weights of 1, and the criticality node weights α are taken as the node importance scores. Through ablation analysis, the node importance score weights were determined to be set equally to 0.25, and the coverage radius r , and minimum redundancy R_{min} to 1 and 2, respectively.

A. Detection Performance Against ML Baselines

Table II presents the test performance of various models across the test cases. The evaluated models are graph-based models, including GCNs, graph attention networks (GATs), Graph Sample and Aggregate (GraphSAGE), GTNs, graph diffusion networks (GDNs), PIGCNs, PIGDNs, and the proposed PIGTN. Physics-informed variants (PIGCN, PIGDN, and PIGTN) ensured that every training sample satisfied the AC-power flow equations (Kirchhoff's laws). Therefore, the additional physics-based loss term added to the original loss function constrained the output to satisfy the physics-driven laws. In the event of an attack, the subsets of measurements attributed to any type of the attacks investigated, imposed large AC-residuals. Consequently, these models retained the near-zero FPR of the base graph network, and recovered much higher TPR, pushing F1-score and overall accuracy to the top across all test cases. Embedding Kirchhoff's laws acted as an inductive prior that suppressed the large AC residual patterns and allowed the network to generalize across different grid sizes and attack types. It substantiated the reason as to why the PIGCN and PIGTN were performing the best relative to the plain graph-based models. In fact, averaged across all seven tested power network topologies, PIGTN reached ACC ≈ 0.933 , F1-score ≈ 0.928 , with TPR ≈ 0.865 , and FPR ≈ 0.0023 , versus the best non-physics baseline here, GraphSAGE at ACC ≈ 0.9146 , F1-score ≈ 0.9057 , TPR ≈ 0.8326 , and FPR ≈ 0.0033 . More specifically, the performance improvements in the proposed PIGNN-based (physics + topology-aware models) attack detectors compared to the other graph-based/topology-aware models (GraphSAGE, GAT, GTN, GCN, and GDN) for different bus system cases are listed as follows:

- In the **14** bus system, PIGTN offered performance improvements of 2.3%–17.4% in ACC, 4.3%–30.9% in TPR, and 2.6%–22.2% in F1-score.

TABLE II: Test-set performance of models across different bus system cases.

Case	Metric	GraphSAGE	GAT	GCN	GDN	GTN	PIGCN	PIGDN	PIGTN
Case 14	ACC	<u>0.927</u>	0.776	0.871	0.883	0.829	0.922	0.842	0.950
	PREC	0.994	0.933	0.989	0.991	1.000	0.994	0.990	0.997
	TPR	0.860	0.594	0.750	0.772	0.658	0.849	0.690	0.903
	FPR	0.0054	0.042	0.008	0.007	0.000	0.005	0.0069	0.0023
	F1	0.922	0.726	0.853	0.868	0.794	0.916	0.814	0.948
Case 30	ACC	<u>0.886</u>	0.761	0.851	0.876	0.754	0.873	0.830	0.897
	PREC	0.989	0.994	0.982	0.987	0.999	0.991	0.999	0.991
	TPR	0.780	0.524	0.713	0.762	0.509	0.753	0.661	0.801
	FPR	0.0083	0.0031	0.012	0.010	0.0004	0.007	0.001	0.0075
	F1	0.873	0.687	0.827	0.860	0.674	0.855	0.795	0.886
Case IEEE 30	ACC	0.886	0.687	0.818	0.817	0.780	<u>0.910</u>	0.857	0.930
	PREC	0.991	0.998	0.999	0.996	1.000	0.996	0.987	0.994
	TPR	0.779	0.375	0.637	0.636	0.560	0.823	0.723	0.865
	FPR	0.0068	0.0008	0.0002	0.0025	0.000	0.0037	0.0093	0.0052
	F1	0.873	0.546	0.778	0.817	0.718	0.901	0.835	0.925
Case 39	ACC	<u>0.994</u>	0.972	0.930	0.934	0.985	0.987	0.985	0.995
	PREC	0.999	1.000	0.998	0.998	1.000	1.000	1.000	1.000
	TPR	0.989	0.944	0.861	0.870	0.971	0.973	0.969	0.989
	FPR	0.0002	0.00	0.0017	0.0021	0.000	0.000	0.000	0.000
	F1	0.994	0.971	0.925	0.929	0.985	0.986	0.984	0.995
Case 57	ACC	0.894	0.851	0.867	0.817	0.807	<u>0.911</u>	0.859	0.931
	PREC	0.999	0.983	0.998	0.999	0.999	1.000	0.999	0.999
	TPR	0.789	0.714	0.736	0.635	0.614	0.822	0.718	0.861
	FPR	0.0004	0.0123	0.0014	0.0004	0.0002	0.000	0.0002	0.0002
	F1	0.882	0.827	0.847	0.776	0.760	0.902	0.836	0.925
Case 118	ACC	<u>0.907</u>	0.811	0.794	0.892	0.547	0.873	0.853	0.911
	PREC	0.999	0.975	0.999	0.997	1.000	1.000	0.999	0.999
	TPR	0.814	0.637	0.588	0.786	0.093	0.746	0.706	0.823
	FPR	0.001	0.0164	0.0002	0.0021	0.000	0.000	0.001	0.0008
	F1	0.897	0.771	0.740	0.879	0.171	0.855	0.827	0.903
Case 200	ACC	<u>0.908</u>	0.903	0.817	0.883	0.654	0.885	0.845	0.919
	PREC	0.999	0.994	0.999	0.999	1.000	1.000	0.999	0.999
	TPR	0.817	0.808	0.634	0.765	0.309	0.769	0.691	0.829
	FPR	0.001	0.0031	0.0004	0.0004	0.000	0.000	0.006	0.0003
	F1	0.899	0.892	0.776	0.867	0.472	0.870	0.817	0.917

- In the **30** bus system, PIGTN offered performance improvements of 1.1%–14.3% in ACC, 2.1%–29.2% in TPR, and 1.3%–21.2% in F1-score.
- In the **IEEE 30** bus system, PIGTN offered performance improvements of 4.4%–24.3% in ACC, 8.6%–49% in TPR, and 5.2%–37.9% in F1-score.
- In the **39** bus system, PIGTN offered performance improvements of 0.1%–6.5% in ACC, 0%–12.8% in TPR, and 0.1%–7% in F1-score. Notably, most models performed well, due to the moderate topological complexity and feature variability of this case.
- In the **57** bus system, PIGTN offered performance improvements of 3.7%–12.4% in A.CC, 7.2%–24.7% in TPR, and 4.3%–16.5% in F1-score.
- In the **118** bus system, PIGTN offered performance improvements of 0.4%–36.4% in ACC, 0.9%–73% in TPR, and 0.6%–73.2% in F1-score.
- In the **200** bus system, PIGTN offered performance improvements of 1.1%–26.5% in ACC, 1.2%–52% in TPR, and 1.8%–44.5% in F1-score.

The added AC power flow loss constraints, forces hidden states to abide by Kirchhoff’s laws by penalizing mismatches in P and Q . Attacks that locally tamper with the measurements while leaving global power-flow relations inconsistent produce larger AC residuals, where the model learns such correlations as these inconsistencies are separable from normal variability.

B. Benchmarking Sensor Placement Strategies

The evaluation carried out presents the improvement gain over the baseline for the GA-PIGTN framework and the benchmark placement methods, namely: (i) the greedy placement method, which selects the top buses based on their importance score, and (ii) the sparse placement method by Yildiz & Abur [13], which is designed to yield the best possible locations for installing a limited number of PMUs to optimize their utility for model-based sparse estimation methods, provided that the baseline represents the existing sensing infrastructure. Table III and Fig. 1 show that GA placements presented more distributed and diverse sensor layouts compared to benchmark methods. It explored a broader search space, which shall also explain the superior results in large and structurally diverse networks. Greedy methods tend to cluster sensors at important nodes, while the Yildiz & Abur method is more relevant in model-based detection settings. From the standpoint of detection under nominal operating conditions, Fig. 2 shows that GA-PIGTN placement exhibits varying performance across the test cases: (i) in Case 30, IEEE 30, and 118, the gain is most prominent, with 2.3%–2.8% improvements in ACC, 5.4%–7.3% in TPR, and 2.9%–3.8% in F1-score, (ii) in Case 57, and 200 the improvements are marginal, and (iii) in Cases 14 and 39, slightly negative gains across ACC, TPR, and F1-score were observed.

These results can be explained by the intrinsic characteristics of the systems. Relatively smaller and less complex topologies (e.g., Cases 14, 39, and 57) that have high percentage of load and/or generator buses, inherently provide extensive measurements of active and reactive power–inferred, either directly or through pseudo-measurements. In such scenarios, the incremental contribution of optimized placements is smaller, leading to the modest or mixed gains observed. Case 200, despite being the largest network, also exhibits only marginal detection gains. With a much dense and uniform topology, GA-PIGTN placement added mostly redundant information from the current detection standpoint. On the other hand, Case 118, which is modular with several loosely coupled sub-areas and corridor buses demonstrated a different behavior. It showed noticeable improvements in detection due to its topological structure and heterogeneity. For Cases 30 and IEEE 30, well-connected topology with $\approx 70\%$ load buses and $\approx 17\%$ generator buses, the detection improvement gains were the most prominent. These results emphasized that the benefits of GA-PIGTN placement depend on the structural and functional characteristics of the system that can make additional sensors impactful or redundant to the detection model. Importantly, the GA-PIGTN framework consistently outperformed Greedy and Yildiz & Abur placements by yielding the least negative, more positive, and most prominent gains relative to the baseline sensor layout. This demonstrates the advantage of the joint optimization framework. Additional sensor placements do not necessarily lead to improved performance as meaningful gains are contingent on an effective and purposeful sensor placement, besides accounting for the intrinsic characteristics of the topology as discussed earlier.

On the other hand and across all cases, Table IV consis-

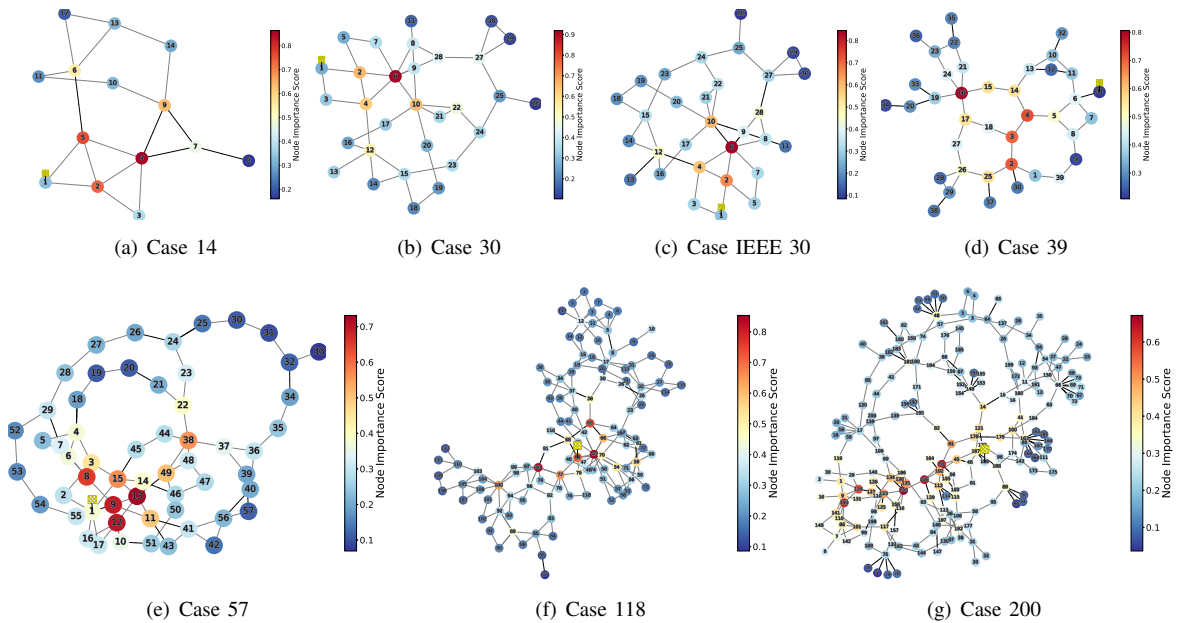


Fig. 1: Graph representations of cases (nodes colored according to computed importance scores).

TABLE III: Sensor placements across test cases.

Placement method	Case 14	Case 30	Case IEEE 30	Case 39	Case 57
Ours	4,5,10,13	3,6,7,9,10,12,15,25,29	3,6,7,9,10,12,15,25,27	1,2,5,6,10,14,15,18,19,22,26	4,7,10,11,14,16,17,22,23,29,32,37,38,48,49,55,56
Greedy	4,5,7,9	4,6–10,12,15,28	4,6,7,9,10,12,15,22,28	2–5,14–18,25,26	4,7,10,11,13–17,22,23,29,37,38,48,49,55
Yildiz & Abur [13]	6	9,13,26,30	26,30	6,8,10,20,28,36	7,33

Placement method	Case 118	Case 200
Ours	2,5,9,11,17,20,23,28,35,37,45,47,48,50,51,57,58,60,63,64,67,68,71,78,79,83,93–98,106,109,118	1,3,7,9,10,14,15,17,22,29,30,36,41,45,46,48,56,61,66,75,81,82,86,89,100–103,107,110,112,113,116–119,121–123,129,131,134,141,142,148,149,156,157,163,178,179–181,184,186–188,192,194,195
Greedy	5,11,17,23,30,35,37,38,45,47,48,50,51,57,58,60,63,64,67–69,71,75,78,79,81–83,94–98,106,118	1,7–10,14,15,29,30,41,45,46,48,55,56,61,66,81,82,86,89,100–103,107,110,112,113,116–119,121–124,128,129,131,133,134,141,142,148,149,156,157,163,178–181,184,186–188,192–195
Yildiz & Abur [13]	32,43,59,73,111,117	2,4,6,8,10,12,13,16,18,–21,23,24,26,28,30,32,33,35,37,38,40,88,162

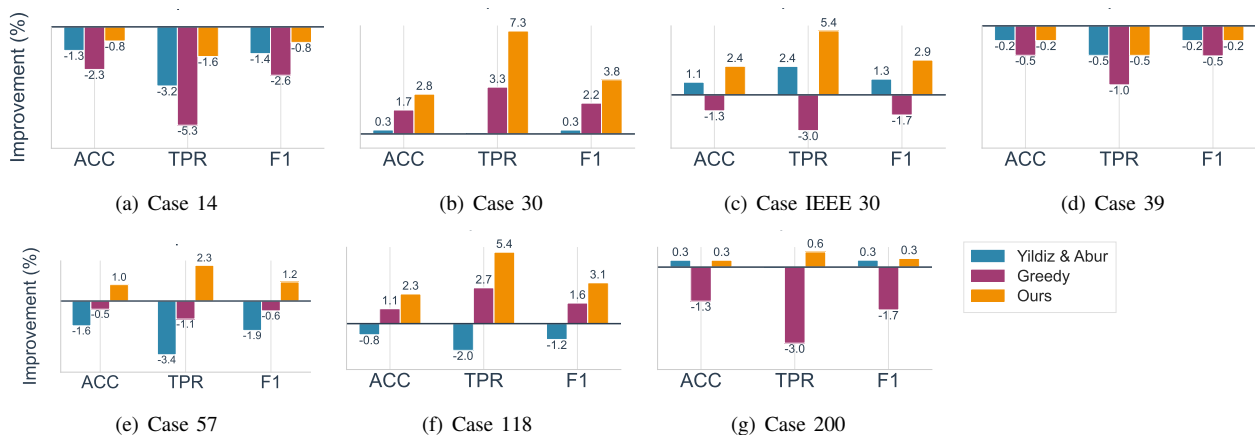


Fig. 2: Detection performance improvement across test cases compared to the baseline.

tently demonstrates the benefits of GA-PIGTN placements in terms of detection robustness. Random sensor failures were simulated that can range up to 30% of the total number of buses. Across smaller and medium-scale systems, GA-

PIGTN provided a clear robustness advantage. In Cases 14, 39, and 57, GA-PIGTN still achieved either the highest or tied-best performance across all performance metrics. Similarly, in Cases 30 and IEEE 30, the GA-PIGTN scored the

TABLE IV: Evaluation on robustness under sensor failures across different bus system cases.

Case	Placement Method	F_{crit}	\mathcal{R}	$\mathcal{A}_{\text{F1-score}}$	$\overline{\text{ACC}}$	$\overline{\text{F1}}$	$\overline{\text{PREC}}$
Case 14	Ours	2	0.907	0.411	0.799	0.822	0.743
	Greedy	2	<u>0.900</u>	<u>0.401</u>	<u>0.776</u>	<u>0.803</u>	<u>0.724</u>
	Yildiz & Abur	2	0.890	0.401	0.766	0.802	0.704
	Baseline	1	0.876	0.397	0.749	0.795	0.681
Case 30	Ours	1	0.851	0.555	0.672	0.740	0.624
	Greedy	1	<u>0.841</u>	<u>0.550</u>	<u>0.673</u>	<u>0.737</u>	<u>0.629</u>
	Yildiz & Abur	1	0.841	0.547	0.666	0.731	0.625
	Baseline	1	0.826	0.535	0.632	0.716	0.591
Case IEEE 30	Ours	2	0.888	0.585	0.747	0.782	0.704
	Greedy	2	0.840	0.568	0.701	0.759	0.647
	Yildiz & Abur	2	0.864	0.581	0.730	0.775	0.681
	Baseline	2	<u>0.867</u>	<u>0.578</u>	<u>0.726</u>	<u>0.774</u>	<u>0.685</u>
Case 39	Ours	3	0.841	0.652	0.769	0.817	0.697
	Greedy	3	0.840	0.647	0.766	0.813	0.694
	Yildiz & Abur	3	<u>0.840</u>	<u>0.651</u>	<u>0.767</u>	<u>0.816</u>	<u>0.697</u>
	Baseline	3	0.828	0.642	0.749	0.804	0.676
Case 57	Ours	2	0.828	0.647	0.694	0.759	0.647
	Greedy	2	0.815	0.651	0.692	0.760	0.641
	Yildiz & Abur	2	<u>0.821</u>	<u>0.645</u>	<u>0.691</u>	<u>0.755</u>	<u>0.642</u>
	Baseline	2	0.803	0.636	0.666	0.746	0.620
Case 118	Ours	13	0.981	0.778	0.836	0.833	0.870
	Greedy	12	0.957	0.776	<u>0.831</u>	0.831	<u>0.846</u>
	Yildiz & Abur	12	<u>0.981</u>	<u>0.778</u>	0.829	<u>0.833</u>	0.841
	Baseline	8	0.922	0.744	0.776	0.797	0.762
Case 200	Ours	16	0.912	0.782	0.800	0.815	0.787
	Greedy	11	<u>0.887</u>	<u>0.778</u>	<u>0.784</u>	<u>0.812</u>	<u>0.750</u>
	Yildiz & Abur	8	0.866	0.758	0.758	0.791	0.720
	Baseline	9	0.880	0.766	0.773	0.799	0.743

highest robustness performance compared to benchmarks. As network scale and connectivity play a critical role, GA-PIGTN placements exploited graph redundancy more effectively in Cases 118 and 200 and resulted in sensor layouts that increased resilience under sensor failures. This was demonstrated by the higher F_{crit} values of 13 and 16 sensors for Cases 118 and 200, respectively. While the GA-PIGTN performance superiority in terms of F_{crit} was only evident in larger cases, the analysis of the remaining robustness metrics presented the following results against the baseline:

- In terms of robustness score (\mathcal{R}) expressed as $\mathcal{R} = 1/(1 + \overline{\Delta\text{ACC}})$, where $\overline{\Delta\text{ACC}}$ is the mean relative accuracy degradation over the failure range, GA-PIGTN showed improved performance by 3.4% as opposed to the greedy and the Yildiz&Abur, which showed 1.3% and 1.5% improvements, respectively.
- In terms of the normalized area under the curve of the F1-score versus failure level (\mathcal{A}_{F1}), GA-PIGTN resulted in improvements by 2.6% vs. 1.4%–1.6% by the placement benchmarks.
- In terms of the average accuracy computed across sensor failure levels ($\overline{\text{ACC}}$), GA-PIGTN demonstrated the best performance with 4.8% improvements, while both greedy and Yildiz&Abur showed 3% improvements.
- In terms of the average F1-score ($\overline{\text{F1}}$), GA-PIGTN resulted in improvements by 2.6% vs. 1.3%–1.6% by the placement benchmarks.
- In terms of the average precision ($\overline{\text{P}}$), GA-PIGTN resulted in improvements by 6.5% vs. 3.2%–3.7% by the

placement benchmarks.

Taken together, even when detection accuracy gains are not significant, GA-PIGTN placements strengthen the resilience of the detection framework under stress conditions. Specifically, (i) in heterogeneous topologies, optimized placements added discriminative coverage and boosted accuracy; (ii) in uniformly structured, highly observable networks, added sensors were mostly redundant, improving robustness more than accuracy, and (iii) with moderate or imbalanced observability, GA-PIGTN bridges coverage gaps most effectively, resulting in significant gains.

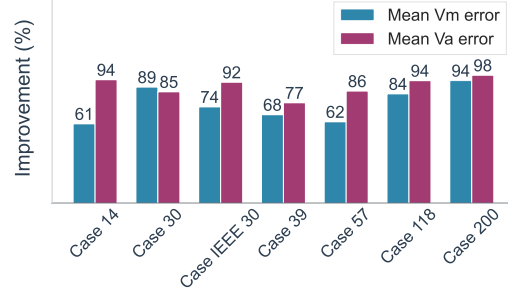


Fig. 3: PSSE performance improvement across test cases.

C. PSSE Performance Analysis

In addition to the enhanced detection performance, the proposed framework led to improved state estimation performance in all test cases. Fig. 3 illustrates the improvement in PSSE performance, measured by the reduction in the mean voltage magnitude (Vm) and voltage angle (Va) errors. The improvement was evaluated on the WLS PSSE. Voltage angle errors showed the greatest improvement (up to 98% improvement), and voltage magnitude errors improved substantially, ranging from 61% to 94%. The proposed framework reinforces a key component of EMSs of power systems.

VI. CONCLUSION

This study presented a joint multi-objective optimization framework for sensor placement and attack detection in power systems using PIGTNs. The framework effectively balanced detection performance and practical sensor placement constraints utilizing NSGA-II for robust layout. It optimized the trade-off between detection performance and sensor placement objectives by placing sensors purposefully. Extensive evaluations of seven test cases confirmed its consistent detection improvements and robustness to sensor failures, compared to sensor placement benchmarks. Its performance gains in TPR and F1-score were achieved without compromising FPR. Moreover, integrating AC power flow constraints into the model loss and co-optimizing sensor placement led to strong generalization to unseen LR attacks. The optimized sensor layouts led to an improvement in PSSE performance—up to 98% reduction in mean state error. Future directions include factoring in sensor deployment cost, as installation costs vary by location. An adversarial training procedure can be investigated to further improve the robustness of the detection model to more sophisticated perturbations.

REFERENCES

- [1] U.S. Department of Energy, Multiyear plan for energy sector cybersecurity, Available: <https://www.energy.gov/ceser/articles/doe-multiyear-plan-energy-cybersecurity>, [Accessed: 21 May 2025] (2018).
- [2] Z. Chang, S. Liu, X. Xiong, Z. Cai, G. Tu, A survey of recent advances in edge-computing-powered artificial intelligence of things, *IEEE Internet of Things Journal* 8 (18) (2021) 13849–13875.
- [3] S. Tan, J. M. Guerrero, P. Xie, R. Han, J. C. Vasquez, Brief survey on attack detection methods for cyber-physical systems, *IEEE Systems Journal* 14 (4) (2020) 5329–5339.
- [4] Z. Qu, Y. Dong, Y. Li, S. Song, T. Jiang, M. Li, Q. Wang, L. Wang, X. Bo, J. Zang, Q. Xu, Localization of dummy data injection attacks in power systems considering incomplete topological information: A spatio-temporal graph wavelet convolutional neural network approach, *Applied Energy* 360 (2024) 122736.
- [5] O. Boyaci, A. Umunnakwe, A. Sahu, M. R. Narimani, M. Ismail, K. R. Davis, E. Serpedin, Graph neural networks based detection of stealth false data injection attacks in smart grids, *IEEE Systems Journal* 16 (2) (2022) 2946–2957.
- [6] A. Vaswani, N. Shazeer, N. Parmar, J. Uszkoreit, L. Jones, A. N. Gomez, E. Kaiser, I. Polosukhin, Attention is all you need, *Advances in neural information processing systems* 30 (2017).
- [7] A. Shehzad, F. Xia, S. Abid, C. Peng, S. Yu, D. Zhang, K. Verspoor, Graph transformers: A survey, *arXiv preprint arXiv:2407.09777* (2024).
- [8] S. Yun, M. Jeong, R. Kim, J. Kang, H. J. Kim, Graph transformer networks, *Advances in neural information processing systems* 32 (2019).
- [9] M. Raissi, P. Perdikaris, G. E. Karniadakis, Physics-informed neural networks: A deep learning framework for solving forward and inverse problems involving nonlinear partial differential equations, *Journal of Computational physics* 378 (2019) 686–707.
- [10] L. D. McClenny, U. M. Braga-Neto, Self-adaptive physics-informed neural networks, *Journal of Computational Physics* 474 (2023) 111722.
- [11] B. Huang, J. Wang, Applications of physics-informed neural networks in power systems - a review, *IEEE Transactions on Power Systems* 38 (1) (2023) 572–588.
- [12] M. J. Zideh, S. K. Solanki, Physics-informed convolutional autoencoder for cyber anomaly detection in power distribution grids, in: 2024 IEEE Power & Energy Society General Meeting (PESGM), 2024, pp. 1–5.
- [13] T. Yildiz, A. Abur, Sparse PMU placement algorithm for enhanced detection and identification of power grid events, *IEEE Transactions on Power Systems* 40 (2) (2025) 1843–1853.
- [14] M. H. Rezaeian Koochi, P. Dehghanian, S. Esmaeili, PMU placement with channel limitation for faulty line detection in transmission systems, *IEEE Transactions on Power Delivery* 35 (2) (2020) 819–827.
- [15] M. Jamei, R. Ramakrishna, T. Tesfay, R. Gentz, C. Roberts, A. Scaglione, S. Peisert, Phasor measurement units optimal placement and performance limits for fault localization, *IEEE Journal on Selected Areas in Communications* 38 (1) (2020) 180–192.
- [16] M. P. Anguswamy, M. Datta, L. Meegahapola, A. Vahidnia, Holistic fault detection, classification, and localization in adns with optimally placed D-PMUs, *IEEE Transactions on Industry Applications* 61 (1) (2025) 1171–1184.
- [17] M. Jamei, A. Scaglione, C. Roberts, E. Stewart, S. Peisert, C. McParland, A. McEachern, Anomaly detection using optimally placed μ PMU sensors in distribution grids, *IEEE Transactions on Power Systems* 33 (4) (2018) 3611–3623.
- [18] C. Pei, Y. Xiao, W. Liang, X. Han, PMU placement protection against coordinated false data injection attacks in smart grid, *IEEE Transactions on Industry Applications* 56 (4) (2020) 4381–4393.
- [19] W. Xia, D. He, J. Chen, On the PMU placement optimization for the detection of false data injection attacks, *IEEE Systems Journal* 17 (3) (2023) 3794–3797.
- [20] Q. Yang, D. An, R. Min, W. Yu, X. Yang, W. Zhao, On optimal PMU placement-based defense against data integrity attacks in smart grid, *IEEE Transactions on Information Forensics and Security* 12 (7) (2017) 1735–1750.
- [21] N. M. Manousakis, G. N. Korres, P. S. Georgilakis, Taxonomy of PMU placement methodologies, *IEEE Transactions on Power Systems* 27 (2) (2012) 1070–1077.
- [22] B. Gou, R. G. Kavasseri, Unified pmu placement for observability and bad data detection in state estimation, *IEEE Transactions on Power Systems* 29 (6) (2014) 2573–2580.
- [23] M. P. Anguswamy, M. Datta, L. Meegahapola, A. Vahidnia, Optimal micro-PMU placement in distribution networks considering usable zero-injection phase strings, *IEEE Transactions on Smart Grid* 13 (5) (2022) 3662–3675.
- [24] N. H. Abbasy, H. M. Ismail, A unified approach for the optimal PMU location for power system state estimation, *IEEE Transactions on Power Systems* 24 (2) (2009) 806–813.
- [25] B. Gou, Optimal placement of PMUs by integer linear programming, *IEEE Transactions on Power Systems* 23 (3) (2008) 1525–1526.
- [26] K. Chauhan, R. Sodhi, Placement of distribution-level phasor measurements for topological observability and monitoring of active distribution networks, *IEEE Transactions on Instrumentation and Measurement* 69 (6) (2020) 3451–3460.
- [27] S. Chakrabarti, E. Kyriakides, Optimal placement of phasor measurement units for power system observability, *IEEE Transactions on Power Systems* 23 (3) (2008) 1433–1440.
- [28] N. Khanam, M. Rihan, S. Hameed, Robust framework for PMU placement and voltage estimation of power distribution network, *IEEE Access* 13 (2025) 55841–55857.
- [29] R. Bhattacharjee, A. De, A novel bus-ranking-algorithm-based heuristic optimization scheme for PMU placement, *IEEE Transactions on Industrial Informatics* 19 (9) (2023) 9921–9932.
- [30] O. Kosut, L. Jia, R. J. Thomas, L. Tong, Malicious data attacks on the smart grid, *IEEE Transactions on Smart Grid* 2 (4) (2011) 645–658.
- [31] H. Ye, C. Tian, Y. Ge, L. Wu, Revisit optimal PMU placement with full zero-injection cluster and redundancy sharing, *IEEE Transactions on Power Systems* 40 (3) (2025) 2700–2710.
- [32] R. Deng, G. Xiao, R. Lu, H. Liang, A. V. Vasilakos, False data injection on state estimation in power systems—attacks, impacts, and defense: A survey, *IEEE Transactions on Industrial Informatics* 13 (2) (2016) 411–423.
- [33] A. Ayad, H. Farag, A. Youssef, E. El-Saadany, Cyber-physical attacks on power distribution systems, *IET Cyber-Physical Systems: Theory & Applications* 5 (2) (2020) 218–225.
- [34] M. A. Husnoo, A. Anwar, N. Hosseinzadeh, S. N. Islam, A. N. Mahmood, R. Doss, False data injection threats in active distribution systems: A comprehensive survey, *Future Generation Computer Systems* 140 (2023) 344–364.
- [35] A. Takiddin, R. Atat, M. Ismail, O. Boyaci, K. R. Davis, E. Serpedin, Generalized graph neural network-based detection of false data injection attacks in smart grids, *IEEE Transactions on Emerging Topics in Computational Intelligence* 7 (3) (2023) 618–630.
- [36] Z. Chu, O. Kosut, L. Sankar, Detecting load redistribution attacks via support vector models, *IET Smart Grid* 3 (5) (2020) 551–560.
- [37] W. Deng, Z. Xiang, K. Huang, J. Liu, C. Yang, W. Gui, Detecting intelligent load redistribution attack based on power load pattern learning in cyber-physical power systems, *IEEE Transactions on Industrial Electronics* 71 (6) (2024) 6285–6293.
- [38] K. Deb, A. Pratap, S. Agarwal, T. Meyarivan, A fast and elitist multiobjective genetic algorithm: NSGA-II, *IEEE Transactions on Evolutionary Computation* 6 (2) (2002) 182–197.
- [39] B. Khemani, S. Patil, K. Kotecha, S. Tanwar, A review of graph neural networks: concepts, architectures, techniques, challenges, datasets, applications, and future directions, *Journal of Big Data* 11 (1) (2024) 18.
- [40] K. Deb, An efficient constraint handling method for genetic algorithms, *Computer methods in applied mechanics and engineering* 186 (2-4) (2000) 311–338.
- [41] Y. Ma, J. Tang, *Deep learning on graphs*, Cambridge University Press, 2021.
- [42] B. Liu, Z. Li, X. Chen, Y. Huang, X. Liu, Recognition and vulnerability analysis of key nodes in power grid based on complex network centrality, *IEEE Transactions on Circuits and Systems II: Express Briefs* 65 (3) (2018) 346–350.
- [43] S. Wang, W. Lv, J. Zhang, S. Luan, C. Chen, X. Gu, Method of power network critical nodes identification and robustness enhancement based on a cooperative framework, *Reliability Engineering & System Safety* 207 (2021) 107313.
- [44] H. Bai, S. Miao, Hybrid flow betweenness approach for identification of vulnerable line in power system, *IET Generation, Transmission & Distribution* 9 (12) (2015) 1324–1331.
- [45] J. D. Glover, M. S. Sarma, T. J. Overbye, *Power system analysis and design*, Cengage Learning, 2011.